Numerical model for the study of hydrodynamics on bays and estuaries

P. Tabuenca and J. Cardona

A. Samartín

A nonlinear implicit finite element model for the solution of two-dimensional (2-D) shallow water equations, based on a Galerkin formulation of the 2-D estuaries hydrodynamic equations, has been developed. Spatial discretization has been achieved by the use of isoparametric, Lagrangian elements. To obtain the different element matrices, Simpson numerical integration has been applied. For time integration of the model, several schemes in finite differences have been used: the Cranck-Nicholson iterative method supplies a superior accuracy and allows us to work with the greatest time step Δt*; however, central differences time integration produces a greater velocity of calculation. The model has been tested with different examples to check its accuracy and advantages in relation to computation and handling of matrices. Finally, an application to the Bay of Santander is also presented.*

Keywords: finite elements, hydrodynamics, shallow water equations

Introduction

The main purpose of this paper is the prediction of field of velocities and tide movements, which are essential factors for shipping, fishing, and coast protection. The research of suitable solutions to tide propagation and flowing problems has experienced a great advance with the arrival of the computer. Numerical methods development permits the formulation of different efficient hydrodynamic models to compute every tide phenomenon with precision and to handle a great amount of information. One of the advantages of numerical modelling is the quantitative description of flowing to a greater number of points in space and time.

Water volume is a physical system submitted to different external actions (such as gravity, wind, and Coriolis effect) verifying the general laws of fluid mechanics. The answer to the system is the evolution of field of velocities and elevation of the water level. This answer is obtained from the solution of momentum and continuity equations:

$$-\frac{\partial p}{\partial x_k}+\frac{\partial \tau_{ik}}{\partial x_i}+\rho b_k=\frac{D(\rho v_k)}{DT}$$
$$\frac{\partial(\rho v_i)}{\partial x_i}+\frac{\partial \rho}{\partial t}=0 \qquad i,k=1,2,3 \tag{1}$$

Different methods have been formulated for the numerical solution of shallow water equations, the greater part based on the finite differences method. This gives advantages from the point of view of computational efficiency, but some difficulties appear, such as limited flexibility of the mesh and poor satisfaction of the border conditions.

The finite element method (F.E.) allows us to work with variable intervals and no orthogonal meshes, which gives a suitable agreement to the topography. However, a great computational effort is required. The wide ribbon of the computational mesh is one of the most important factors increasing the cost of a F.E. model, while finite difference methods are independent of the model magnitude. It is possible to overcome this difficulty using procedures such as the one described in this paper.

Shallow water equations

The governing equations for homogenous and incompressible fluids are[1]

$$\frac{\partial v_i}{\partial x_i} = 0$$
$$\frac{\partial v_i}{\partial t} + \frac{\partial (v_i v_j)}{\partial x_j} = b_i - \frac{1}{\rho}\frac{\partial p}{\partial x_i} + \frac{1}{\rho}\frac{\partial \tau_{ij}}{\partial x_j} \tag{2}$$

For Newtonian fluids the following relations between strains and deformations exist:

$$\tau_{ij} = 2\mu\epsilon_{ij} = \begin{cases} \mu\left(\frac{\partial v_i}{\partial x_j} + \frac{\partial v_j}{\partial x_i}\right) & i \neq j \\ 2\mu\frac{\partial v_i}{\partial x_j} & i = j \end{cases} \tag{3}$$

These relations allow us to express the stresses τ_{ij} as a function of velocity, obtaining in this way the Navier-Stokes equations,

$$\frac{\partial v_i}{\partial t} + \frac{\partial (v_i v_j)}{\partial x_j} = b_i - \frac{1}{\rho}\frac{\partial p}{\partial x_i} + \frac{\mu}{\rho}\frac{\partial^2 v_i}{\partial x_j^2} \tag{4}$$

Boundary conditions are (*Figure 1*)

$$\left.\begin{aligned} v_n &= \bar{v}_n \\ v_s &= \bar{v}_s \end{aligned}\right\} \quad \text{over } S_1 \tag{5}$$

$$\begin{aligned} -p + \tau_{nn} &= -p + 2\mu\frac{\partial v_n}{\partial n} = \bar{\sigma}_n \\ \tau_{ns} &= \mu\left(\frac{\partial v_n}{\partial s} + \frac{\partial v_s}{\partial n}\right) = \bar{\sigma}_s \end{aligned} \quad \text{over } S_2 \tag{6}$$

S_1 is the surface on which the velocities are specified. If S_1 is a physical border, such as a wall, then the two velocity components are zero.

S_2 is the surface where forces acting over the border are specified; i.e., on a free surface they are pressure and friction of the wind.

The solution of equations (2), together with the corresponding boundary conditions, represents a difficult task. Usually, it is necessary to simplify these equations and to transform them into shallow water equations.

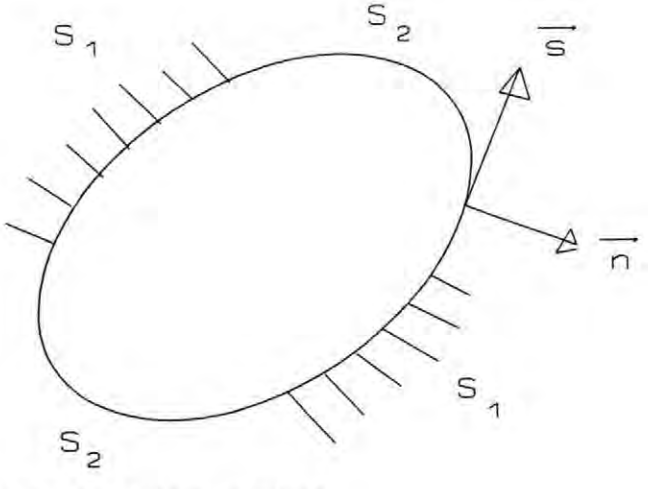

Figure 1. Boundary conditions

For the shallow water case, vertical acceleration and strain terms are negligible except for the pressure and gravity terms. So the existing pressure is the atmospheric pressure, i.e.,

$$p = \rho g(\zeta - z) + p_A \tag{7}$$

Averaging continuity and momentum equations through the sea depth, the equations for hydrodynamics of the estuaries are obtained:

$$\frac{\partial H}{\partial t} + \frac{\partial (HU)}{\partial x} + \frac{\partial (HV)}{\partial y} = 0 \tag{8}$$

$$\frac{\partial U}{\partial t} + U\frac{\partial U}{\partial x} + V\frac{\partial U}{\partial y} - fV + g\frac{\partial \zeta}{\partial x} - \frac{KW^2}{H}\cos\Psi + \frac{gU\sqrt{U^2+V^2}}{HC^2} = 0 \tag{9}$$

$$\frac{\partial V}{\partial t} + U\frac{\partial V}{\partial x} + V\frac{\partial V}{\partial y} + fU + g\frac{\partial \zeta}{\partial x} - \frac{KW^2}{H}\sin\Psi + \frac{gV\sqrt{U^2+V^2}}{HC^2} = 0 \tag{10}$$

where f is the Coriolis parameter, K is a dimensionless coefficient function of the wind velocity W, C is the Chezy coefficient, and Ψ is the angle between the wind velocity vector and the X-axis. The remaining parameters are defined in *Figure 2*.

In order to obtain the values of H, U, and V from equations (8)–(10), boundary and initial conditions must be considered. One of the common difficulties in this class of two-dimensional (2-D) hydrodynamic models is the treatment of boundary conditions at both open and shoreline boundaries. The first type corresponds to open boundaries, for example, river delta or open sea. The second one is related to the fixed boundaries, for example, the coastline.

In the first case the normal velocity v_n, the water surface elevation ζ, or both can be specified as long as the system is not overconstrained. For fixed boundaries the normal flow throughout the coastline is zero ($v_n = 0$). The initial conditions are assumed to be known.

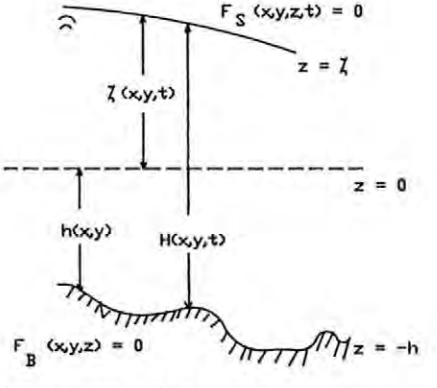

Figure 2. Cross section of an estuary

Finite element model

In the finite element model (FEM), each variable is expanded in terms of a discrete set of functions $\Phi_j(x, y)$ and nodal values $U_j(t)$, $V_j(t)$, $\zeta_j(t)$, as follows:

$$U = \sum_{j=1}^{N} U_j(t) \cdot \Phi_j(x, y)$$

$$V = \sum_{j=1}^{N} V_j(t) \cdot \Phi_j(x, y) \tag{11}$$

$$\zeta = \sum_{j=1}^{N} \zeta_j(t) \cdot \Phi_j(x, y)$$

The rest of the parameters are expanded using the same basic functions Φ_j. These functions are assumed to be polynomial 2-D, and they are selected verifying

1. interelement continuity;
2. $\Phi_i(x_j) = \delta_{ij}$ (with δ_{ij} the Kronecker delta); and
3. $\Phi_i \neq 0$ only over the union of elements containing i node.

Substitution of (11) into (8)–(10) and application of the Galerkin method give the following set of equations:

$$M_{ij}\dot{\zeta}_j = E_{\zeta_i}$$

$$M_{ij}\dot{U}_j = E_{U_i} \tag{12}$$

$$M_{ij}\dot{V}_j = E_{V_i}$$

where

$$E_{\zeta_i} = -(\zeta_j + h_j) \cdot K_{xikj} \cdot U_j - U_k \cdot K_{xikj} \cdot (\zeta_j + h_j) - (\zeta_j + h_j) \cdot k_{yijk} \cdot V_k - V_k \cdot K_{yikj} \cdot (\zeta_j + h_j)$$

$$E_{U_i} = -U_k \cdot K_{xikj} \cdot U_j - V_k \cdot K_{ykj} \cdot U_j + f_k \cdot C_{ijk} \cdot V_j - g \cdot D_{xij} \cdot \zeta_j + E_{ij} \cdot K_j \cdot W_j^2 \cdot \cos\Psi_j - \frac{g}{C^2} \cdot R_{ij} \cdot U_j \tag{13}$$

$$E_{V_i} = U_k \cdot K_{xikj} \cdot V_j - V_k \cdot K_{yijk} \cdot V_j - f_k \cdot C_{ikj} \cdot U_j - g \cdot D_{yij} \cdot \zeta_j + E_{ij} \cdot K_j \cdot W_j^2 \cdot \sin\Psi_j - \frac{g}{C^2} \cdot R_{ij} \cdot V_j$$

with

$$M_{ij} = \int_A \Phi_i \cdot \Phi_j \cdot dA$$

$$k_{xijk} = \int_A \Phi_i \cdot \Phi_j \cdot \frac{\partial \Phi_k}{\partial x} \cdot dA$$

$$k_{yijk} = \int_A \Phi_i \cdot \Phi_j \cdot \frac{\partial \Phi_k}{\partial y} \cdot dA$$

$$C_{ijk} = \int_A \Phi_i \cdot \Phi_j \cdot \Phi_k \cdot dA$$

$$D_{xij} = \int_A \Phi_i \cdot \frac{\partial \Phi_j}{\partial x} \cdot dA$$

$$D_{yij} = \int_A \Phi_i \cdot \frac{\partial \Phi_j}{\partial y} \cdot dA$$

$$E_{ij} = \int_A \frac{\Phi_i \cdot \Phi_j}{\sum (\zeta_k + h_j) \cdot \Phi_k} \cdot dA$$

$$R_{ij} = \int_A \Phi_i \cdot \Phi_j \cdot \frac{\sqrt{\left(\sum U_k \cdot \Phi_k\right)^2 + \left(\sum V_k \cdot \Phi_k\right)^2}}{\sum (\zeta_k + h_k) \cdot \Phi_k} \cdot dA \tag{14}$$

The set (12) of simultaneous first-order differential equations is nonlinear, because the coefficients R_{ij} and E_{ij} depend on the unknowns ζ, U, and V. The remaining coefficients are a function only of the geometry element. Then the problem to deal with is integrating, in the time domain for the nodal values, the system of coupled equations (12). In this respect, besides equations (12), initial conditions must be given, and constraints along the boundary must also be specified.

The spatial discretization has been carried out by quadratic Lagrangian elements. These elements are obtained from isoparametric transformation from square "parent" elements, as is shown in *Figure 3*. In this way their curved borders allow us to adapt the finite element mesh to the domain considered. The isoparametric transformation allows us to simplify matrix calculation because it is made over the element $\hat{A}$ with right sides on the ξ, η plane. For spatial integration the Simpson integration formula for nine points is applied.[2] In this way, integration points coincide with

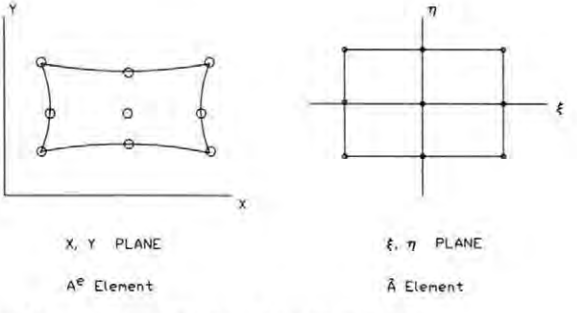

Figure 3. Quadratic element transformation

interpolation nodes, and set (12) becomes

$$M_i\dot{\zeta}_i = E_{\zeta_i} \qquad M_i\dot{U}_i = E_{U_i} \qquad M_i\dot{V}_i = E_{V_i} \tag{15}$$

with

$$\begin{aligned}
E_{\zeta_i} &= -k_{xik}[(\zeta_i + h_i)\cdot U_k + (\zeta_k + h_k)\cdot U_i] - (k_{yik}[(\zeta_i + h_i)\cdot V_k + (\zeta_k + h_k)\cdot V_i \\
E_{U_i} &= -k_{xik}[\cdot U_i\cdot U_k + g\zeta_k] - k_{yik}V_i\cdot U_k + C_i\cdot f_i\cdot V_i + E_i\cdot K_i\cdot W_i^2\cdot\cos\Psi_i - \frac{g}{C^2}\cdot R_i\cdot U_i \\
E_{V_i} &= -k_{xik}\cdot U_i\cdot V_k - k_{yik}[V_i\cdot V_k + g\zeta_k] - C_i\cdot f_i\cdot U_i + E_i\cdot K_i\cdot W_i^2\cdot\sin\Psi_i - \frac{g}{C^2}\cdot R_i\cdot V_i
\end{aligned} \tag{16}$$

For the integration in time, two alternative procedures have been used:

Cranck-Nicholson procedure.[3] The time derivatives are approximated by the trapezoidal formula, obtaining the solution by the expressions

$$\begin{aligned}
\zeta_i(t+\Delta t) &= \zeta_i(t) + \frac{\Delta t}{2M_i}[E_{\zeta_i}(t) + E_{\zeta_i}(t+\Delta t)] \\
U_i(t+\Delta t) &= U_i(t) + \frac{\Delta t}{2M_i}[E_{U_i}(t) + E_{U_i}(t+\Delta t)] \\
V_i(t+\Delta t) &= V_i(t) + \frac{\Delta t}{2M_i}[E_{V_i}(t) + E_{V_i}(t+\Delta t)]
\end{aligned} \tag{17}$$

Given ζ_i, U_i, V_i at time t, the solution at $t + \Delta t$ is obtained iteratively.

Central differences procedure.[4] In this case, solutions are approximated as follows:

$$\begin{aligned}
\zeta_i(t+\Delta t) &= \zeta_i(t-\Delta t) + \frac{2\Delta t}{M_i}\cdot E_\zeta(t) \\
U_i(t+\Delta t) &= U_i(t-\Delta t) + \frac{2\Delta t}{M_i}\cdot E_U(t) \\
V_i(t+\Delta t) &= V_i(t-\Delta t) + \frac{2\Delta t}{M_i}\cdot E_V(t)
\end{aligned} \tag{18}$$

In the two above step-by-step procedures the initial conditions are used as starting values.

Interval Δt is limited by the Courant condition,

$$\Delta t \le \frac{\Delta L}{\sqrt{gH}} \tag{19}$$

where ΔL is the characteristic length of the element.

The iterative procedure gives more accurate results than the central differences procedure; however, it demands more CPU time, because it must be iterated at each time step Δt for obtaining the solution. For the iterative procedure the solution must be known at times $t + \Delta t$ and t.

By using either of the two procedures the set of differential equations is transformed into the following set of equations:

$$\begin{aligned}
\zeta_i(t+\Delta t) &= R_{\zeta_i} \\
U_i(t+\Delta t) &= R_{U_i} \\
V_i(t+\Delta t) &= R_{V_i}
\end{aligned} \tag{20}$$

where $R_{\zeta i}$, R_{Ui}, and R_{Vi} are the right-hand members of (17) or (18).

In order to solve (15) it is necessary to consider the boundary conditions. Then the specified values of ζ, U, and V must be introduced into the analysis at each time interval along the border. At i nodes with normal velocity V_{ni} imposed, U_i and V_i are approximated as follows:[5]

$$\begin{aligned}
U_i(t+\Delta t) &= \sin^2\theta_i\cdot R_{Ui} - \sin\theta_i\cdot\cos\theta_i\cdot R_{Vi} + \cos\theta_i\cdot V_{ni} \\
V_i(t+\Delta t) &= -\cos\theta_i\cdot\sin\theta_i\cdot R_{Ui} - \cos^2\theta_i\cdot R_{V_i} + \sin\theta_i\cdot V_{ni}
\end{aligned} \tag{21}$$

where θ_i is the made angle between the X-axis and the normal direction that allows us to perform calculation in a direct way.

Numerical tests

First, in order to test the model, it has been applied to three simple cases. Cases 1 and 2 have been solved previously by several authors using different methods; case 3 has a closed form solution. In this way the efficiency and degree of accuracy of the numerical method used can be checked.

Case 1. Rectangular lake. This corresponds to the study of the circulation in a large rectangular lake with dimensions 125,000 × 31,250 m and h = 80 m depth. Tides are not considered, and the circulation is due to the wind only, with posterior influence of the Coriolis effect. This problem has been solved by another method.[6] The comparison between results obtained by both methods are shown in Table 1. The data are eolic coefficient K = 1, wind velocity W = 10 m/s at axis X direction, Coriolis factor f = 10 s^{-1}, and Chezy coefficient C = 10 $m^{1/2}/s$. At the border, V_n has been imposed. The FEM mesh used to find the numerical solution is also shown in *Figure 4*. It is composed of five elements and 33 nodes. The time interval used is

Table 1. Comparison of results

t (*sg*)	*E.F. velocity* (*m*)	*Calculated velocity*[3] (*m*)
1,000	$+1{,}0650 \times 10^{-3}$	$+1{,}0645 \times 10^{-3}$
2,000	$+1{,}0910 \times 10^{-3}$	$+1{,}1613 \times 10^{-3}$
3,000	$+1{,}1610 \times 10^{-3}$	$+1{,}0645 \times 10^{-3}$
4,000	$+0{,}6900 \times 10^{-3}$	not calculated
5,000	$0{,}7248 \times 10^{-3}$	not calculated
6,000	$-1{,}2310 \times 10^{-3}$	$-1{,}1129 \times 10^{-3}$
7,000	$-1{,}0800 \times 10^{-3}$	$-1{,}1613 \times 10^{-3}$
8,000	$-0{,}9825 \times 10^{-3}$	not calculated
9,000	$+2{,}7450 \times 10^{-3}$	not calculated
10,000	$+1{,}1440 \times 10^{-3}$	$+1{,}0645 \times 10^{-3}$

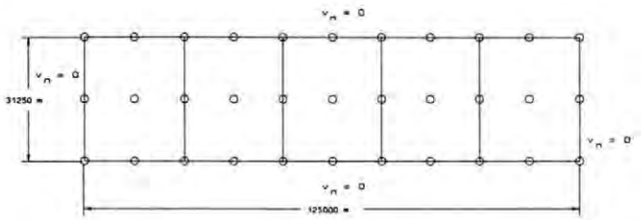

Figure 4. Rectangular lake. Finite element mesh

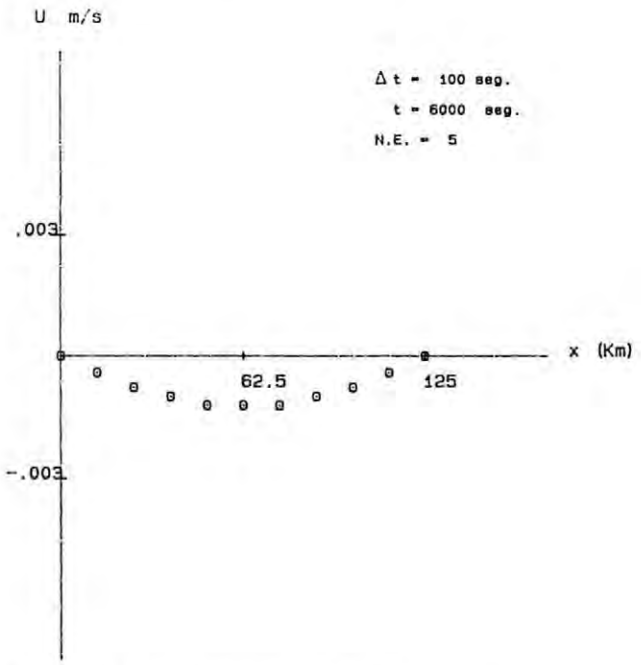

Figure 5. Rectangular lake. $U(x)$ at $t = 6000$ s

$\Delta t = 100$ s. *Figures 5* and *6* show the graphic representations of U as a function of x at the instant $t = 6000$ s and U as a function of t for $x = 62{,}500$ m, respectively. Finally, *Figure 7* gives the contour lines where the Coriolis effect is evident.

Case 2. Rectangular bay. This is a rectangular bay shown in *Figure 8* with dimensions 36,000 × 55,000 m and 36 m depth. The bay entrance is located at the west of the northern border, and its length is 18,000 m. The

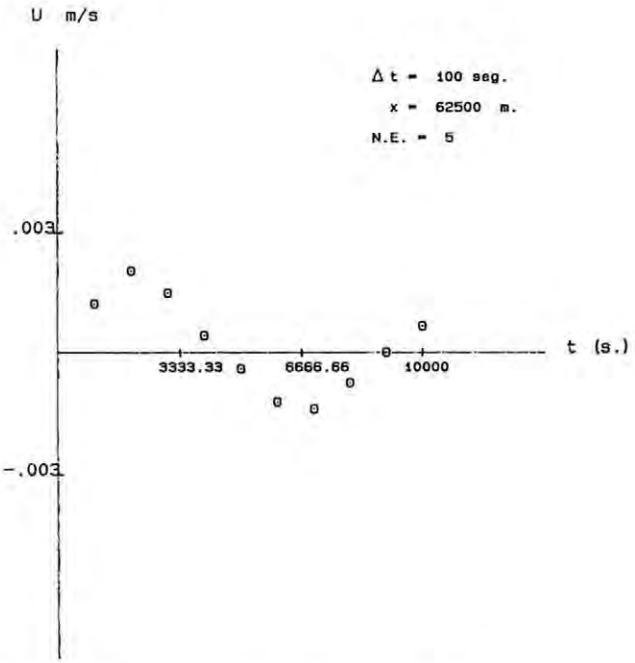

Figure 6. Rectangular lake. $U(t)$ at $x = 62{,}500$ m

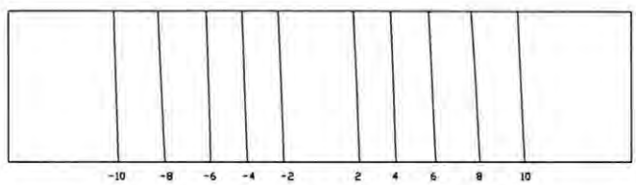

Figure 7. Rectangular lake. Contour lines (mm) at $t = 5000$ s

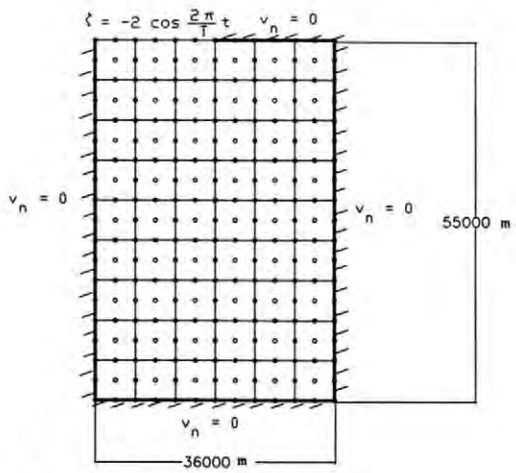

Figure 8. Rectangular bay. E.F. mesh

finite element mesh used has 54 elements and 247 nodes. Tide amplitude is 2 m, period $T = 12.4$ hr, the Chezy coefficient $C = 10\ m^{1/2}/s$, and $\Delta t = 20$ s. This problem has been solved[7] and comparison with the obtained results shows the validity of this method in 2-D.

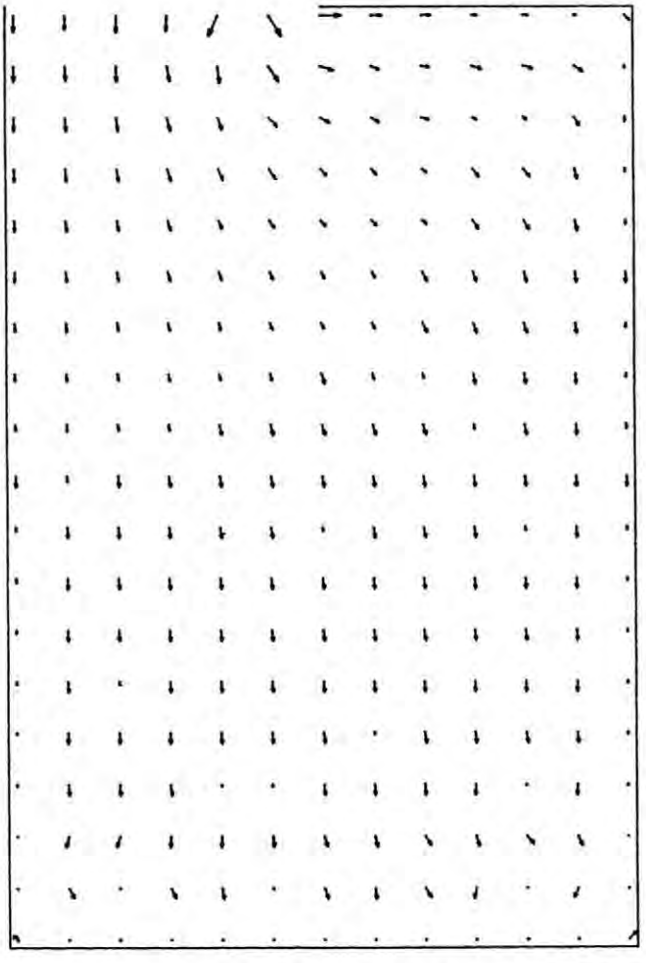

Figure 9. Rectangular bay. Field of velocities at $t = 20{,}000$ s

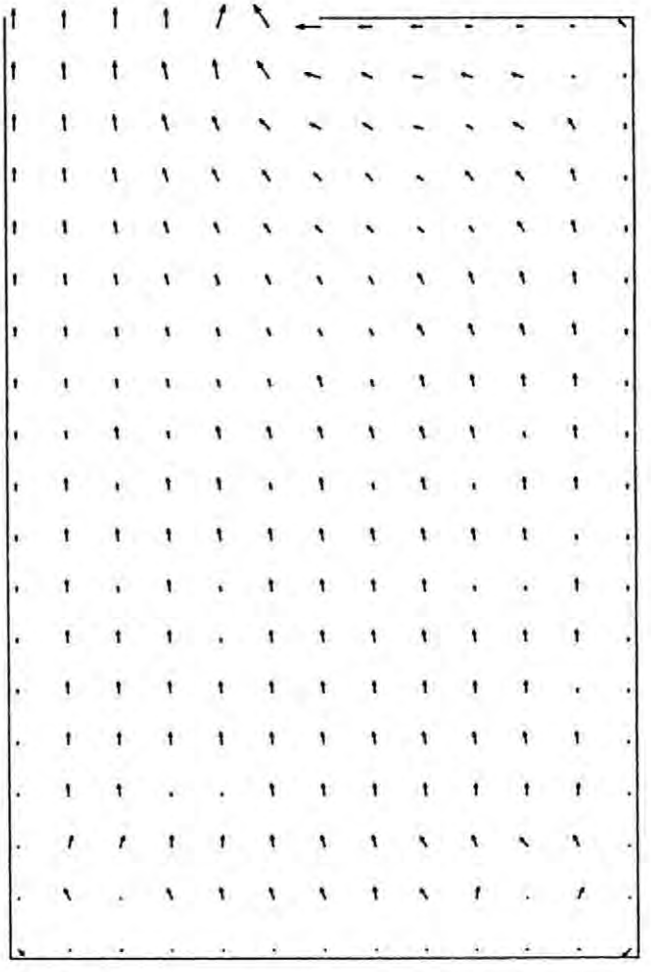

Figure 10. Rectangular bay. Velocities field at $t = 40{,}000$ s

The results for the velocity field are shown in *Figures 9* and *10* at $t = 20{,}000$ s and $t = 40{,}000$ s, respectively.

Case 3. Closed rectangular channel. Water elevation and evolution of the velocity field have been obtained for the channel in *Figure 11* with $h = 9.81$ m depth. There is no wind, and the Coriolis effect is neglected. Initial conditions are null, and period $T = 2\pi$ s. The solution obtained for ζ and U as a function of x at $t = 4.7112$ s with interval $\Delta t = 0.3926$ s, without friction on the bottom, is shown in *Figures 12* and *13* and compared with the analytical solution ζ, $u = 1.0 \sin (t - x/9.81)$. Only the interval corresponding to the progressive wave has been considered, and the discordance between the transitory F.E. solution and the stationary analytical solution at points with $x > 40$ m is due to the fact that these points are not reached by the wave at this time. The experimentation with Δt lower or a larger number of elements has not affected the results obtained. In the same way this problem has been solved for long waves with $T = 20\pi$ s. Without friction ($C = 10^{-20}$ m$^{1/2}$ s^{-1}), unstable solutions had been observed. Increasing the friction term causes instability to disappear. For $C = 1$ m$^{1/2}$ s^{-1} the solution is shown in *Figure 14* beside the analytical solution without friction. It has been verified that the F.E. solution tends toward the stationary solution for growing Chezy coefficients.

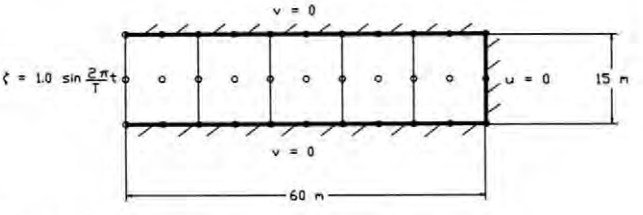

Figure 11. Closed rectangular channel

Application to the Bay of Santander

The model has been applied to the Bay of Santander (Spain). The geometry of this bay is shown in *Figure 15*, and the data for different sea depths has been obtained from Junta del Puerto (Harbour Authorities) charts. The FEM mesh used in this study is composed of 77 elements and 355 nodes. In this problem the

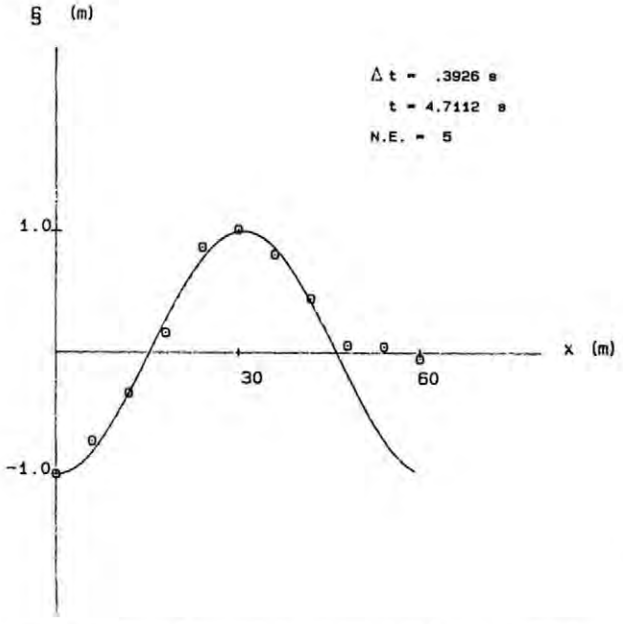

Figure 12. Closed rectangular channel. $\zeta(x)$ at $t = 4.7112$ s

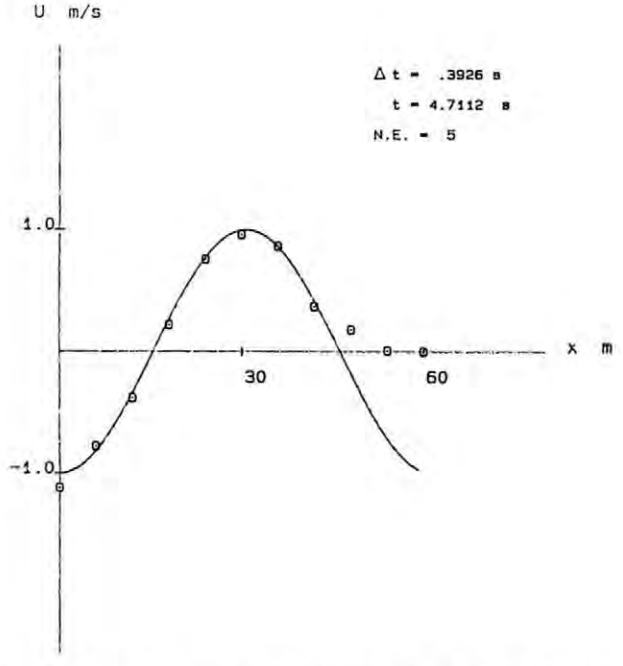

Figure 13. Closed rectangular channel. $U(x)$ at $t = 4.7112$ s

following additional data have been used: eolic coefficient $K = 10^{-5}$, wind velocity $W = 3.0$ m/s at $\Psi = \pi/4$, Chezy coefficient $C = 5.0$ m$^{1/2}$/s, and Coriolis factor $f = 0$. The imposed boundary conditions are:

1. north border nodes level: $\zeta = -2.0 \cos(2\pi/44640)t$
2. south nodes: $v = 0$
3. land border: $v_x = 0$

Some illustrative results are given in *Figures 16* and

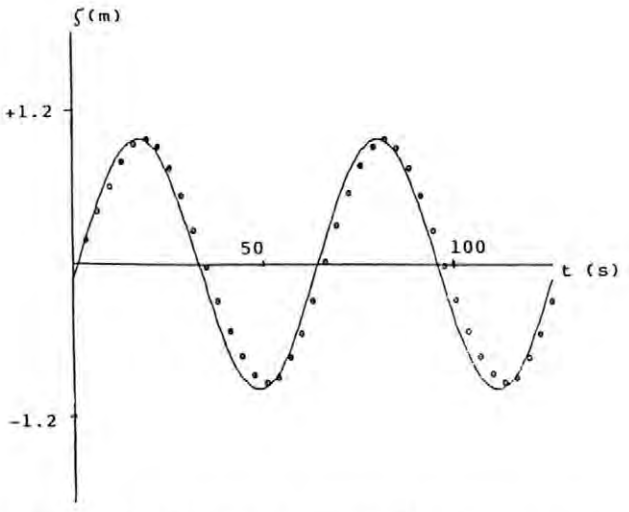

Figure 14. Closed rectangular channel. Long waves. $\zeta(t)$ at $x = 12$ m. $C = 1$ m$^{1/2}$/s

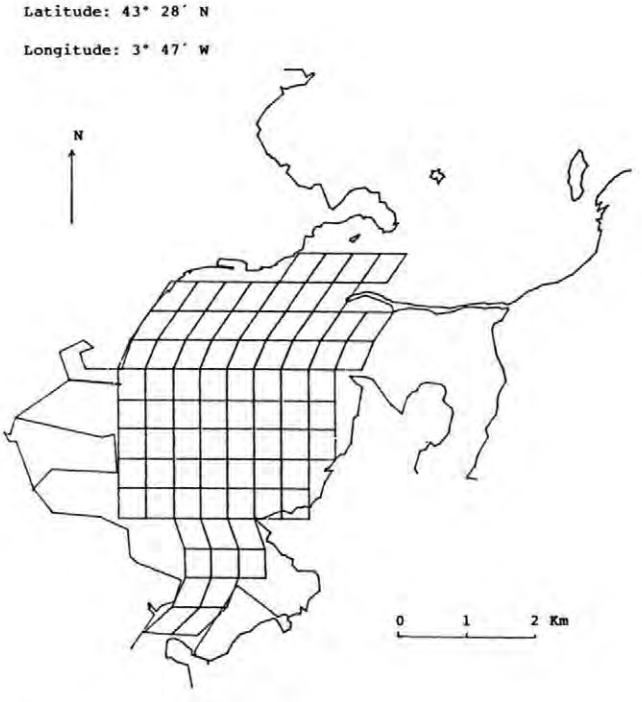

Figure 15. Santander Bay. Finite element mesh

17, where the velocity field at $t = 20{,}000$ s (flood tide) and at $t = 30{,}000$ s (ebb tide) are shown.

It has been observed that for Chezy coefficients $C \geq 20$ m$^{1/2}$/s the model becomes unstable. However, it is possible to overcome this difficulty, starting the model with low coefficients and changing later with the above coefficient.

Conclusions

In the application of the model just described the following conclusions have been reached:

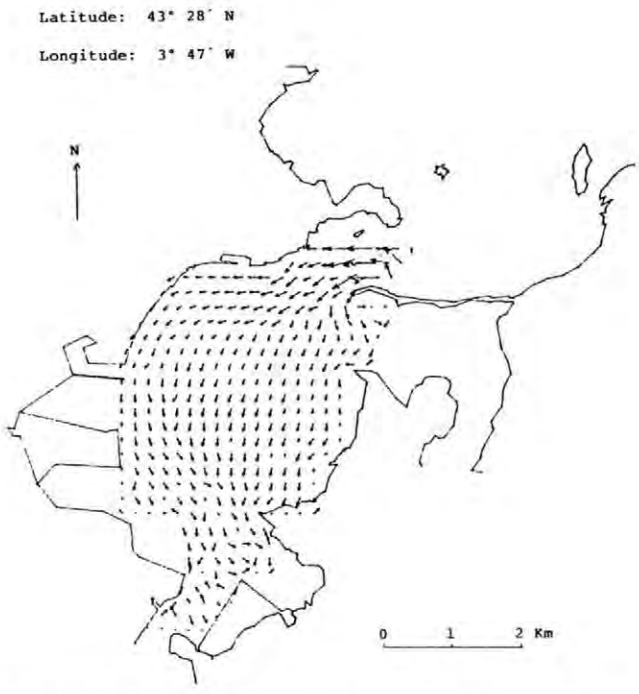

Figure 16. Santander Bay. Field of velocities at $t = 20{,}000$ s

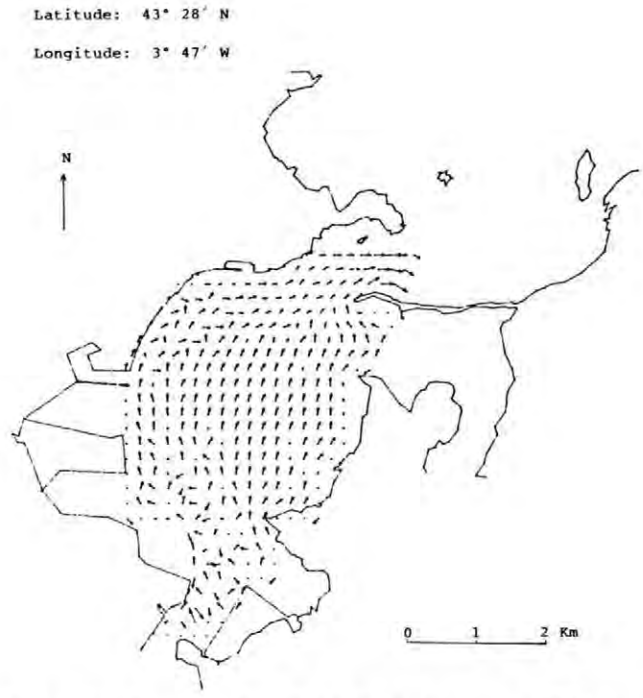

Figure 17. Santander Bay. Field of velocities at $t = 30{,}000$ s

The Simpson spatial integration scheme used simplifies the construction of the global array of equations and reduces the computation of the element matrix to a formula of a point.

The application of the model to problems with a great number of nodes or small time step ($\Delta t \ll T$) demands the use of high-speed computers.

This model is comparable to finite differences methods from the point of view of computational efficiency.

Several parameters (friction terms, eolic coefficient, etc.) are of vital importance in the stability and accuracy of the model. It is necessary to include dissipative nonlinear terms, because their elimination may produce unstable solutions.

Solutions on the southern side of the Bay of Santander are improved when the computer runs several tide cycles.

References

1 Pritchard, D. W. Dispersion and flushing of pollutants in estuaries. *J. Hydraul. Div. Am. Soc. Civil Eng.* 1969, **95**(HY1)

2 Stoer, J. and Bulirsch, R. *Introduction to Analysis*. Springer-Verlag, New York, 1980

3 Smith, A. S., Siemienich, J. L., and Gladwell, I. Evaluation of Norsett methods for integrating differential equations in time. *Int. J. Numer. Anal. Meth. Geomech.* 1977, **10**, 57–73

4 Zienkiewick, O. C. *Finite Element and Approximation*. Wiley-Interscience, New York, 1983

5 Tabuenca, P. and Cardona, J. Modelo de circulación de corrientes basado en el método de los elementos finitos. Aplicación a la Bahía de Santander.-X Congresso Ibero-Latino-Americano sobre Métodos Computacionais em Engenharia. II Encontro Nacional de Mecánica Computacional, I Vol. 3, pp. B-49, B-63, Porto, Portugal, Sept. 25–27, 1989

6 Taylor, C. and Davis, J. M. Tidal propagation and long wave propagation: A finite element approach. *Comput. Fluids* 1975, **3**, 125–148

7 Gray, W. G. An efficient finite element scheme for two-dimensional surface water computation. *Finite Element in Water Resources*. Pentech Press, Plymouth, Mass., 1977